Université de Mons
**Faculté Polytechnique – Service de Mécanique Rationnelle, Dynamique et Vibrations**
31, Bld Dolez - B-7000 MONS (Belgique)
065/37 42 15 – georges.kouroussis@umons.ac.be

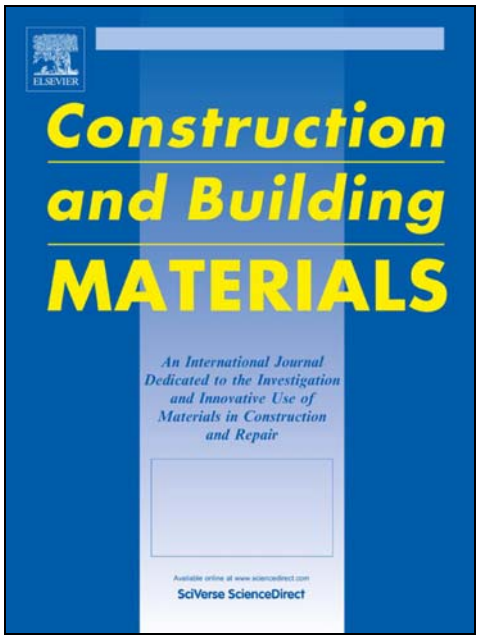


D. López-Mendoza, D. P. Connolly, A. Romero, G. Kouroussis, P. Galvín, A transfer function method to predict building vibration and its application to railway defects, *Construction and Building Materials*, 232, 117217, 2020.

Construction and Building Materials 232 (2020) 117217

Contents lists available at ScienceDirect

Construction and Building Materials

journal homepage: www.elsevier.com/locate/conbuildmat

# A transfer function method to predict building vibration and its application to railway defects

D. López-Mendoza [a], D.P. Connolly [b], A. Romero [a], G. Kouroussis [c], P. Galvín [a,*]

[a] Escuela Técnica Superior de Ingeniería, Universidad de Sevilla, Camino de los Descubrimientos s/n, 41092 Sevilla, Spain
[b] Institute for High Speed Rail and Systems Integration, School of Civil Engineering, University of Leeds, UK
[c] Faculty of Engineering, Department of Theoretical Mechanics, Dynamics and Vibrations, Université de Mons, Belgium

## HIGHLIGHTS

- Simplified method to evaluate building shaking due to arbitrary base excitations.
- Soil-structure transfer functions combined with free-field response are used to estimate building vibration.
- The newly proposed approach obtains the result instantly.
- The method can be used to estimate the vibration in buildings, accounting for SSI and floor amplification.
- Local track defects are shown to have a strong influence on building vibrations.

## ARTICLE INFO

*Article history:*
Received 11 April 2019
Received in revised form 14 September 2019
Accepted 10 October 2019

*Keywords:*
Ground-borne vibrations
Railway traffic
High speed rail
Building vibrations
Structural vibration
Environmental Impact Assessment (EIA)
Railway singular defects

## ABSTRACT

This work presents a simplified method to evaluate building shaking due to arbitrary base excitations, and an example application to railway problems. The model requires minimal computational effort and can be applied to a wide range of footing shapes, thus making it attractive for scoping-type analysis. It uses the soil excitation spectrum at the building footing location as it's input, and computes the building response at any arbitrary location within it's 3D structure. To show an application of the model versatility, it is used to compute building response due to a variety of singular railway defects (e.g. switches/crossings). It is however suitable for more general applications including railway problems without defects. The approach is novel because current railway scoping models do not use soil-structure transfer functions combined with free-field response to estimate building vibration by railway defects. First the soil-structure interaction approach is outlined for both rigid and flexible footings. Then it is validated by comparing results against a comprehensive fully-coupled 3D FEM-BEM model. Finally, it is used to analyse the effect of a variety of variables related to railway defects on building response. Local track defects are shown to have a strong influence on building vibrations. Further, vibration levels close to the threshold of human comfort are found in buildings close to the railway line. Overall the new approach allows for the computation of building vibrations accounting for soil-structure interaction, floor amplification and the measured/computed free-field response due to railway traffic using minimal computational effort.



## 1. Introduction

The response of structures to ground-borne waves induced by blasting, earthquakes, roads and railway traffic, are examples of where soil-structure interaction (SSI) is an important issue [1,2].

This was addressed by Wu and Hao [3,4] who investigated blast-induced ground excitation. They proposed a numerical model to predict surface ground motion due to underground blasting. The free-field response was used as an input to obtain the building response using a simple approach, where the source (blasting)-receiver (building) interaction was neglected. Alternatively, Bayraktar et al. [5] developed a detailed nonlinear dynamic model to simulate concrete and masonry structures using an hybrid approach. Ground excitations due to blasting were measured and combined with a numerical building model, informed using experimental dynamic characteristics. Dogan et al. [6] also presented a combined experimental/numerical procedure to obtain building

* Corresponding author.
*E-mail address:* pedrogalvin@us.es (P. Galvín).

https://doi.org/10.1016/j.conbuildmat.2019.117217
0950-0618/

response due to blasting. Ground motion was measured while building vibration was computed using a 3D model ignoring SSI. A comparison between underground and surface blasting was made and it was found that vibrations were lower for the underground case.

Alternatively, the effect of SSI on the seismic response of buildings in soft layered soils was analysed by Savin et al. [7], using a detailed 3D model. Also, Gatti et al. [8] presented a complete approach to model the full path from the source (earthquake) to a nuclear reactor. To do so, wave-motion was used as an input for a SSI boundary element (BEM)- finite element (FEM) model. Alternatively, simplified procedures [9–11] have been proposed to model SSI for seismic applications.

Numerical models to compute building vibrations due to road traffic include Pyl et al. [12,13] who presented a coupled BEM-FEM methodology to analyse the road-soil-structure system. Alternatively, François et al. [14] studied dynamic building behaviour considering the relative stiffness between the building and the soil, with the aim of simplifying soil-structure interaction.

Regarding the rail sector, the growth of urban railway track infrastructure has led to an increase in the number of properties affected by ground-borne railway vibrations [15–19]. The negative effects caused by railway traffic are more prominent in the presence of local irregularities [20] and are addressed in international standards [21–23]. Thus, it is desirable to estimate the potential increase in vibrations levels in nearby buildings.

To do so, a variety of numerical models have been proposed to compute building induced vibrations due to railway traffic. Prior to the construction stage of a new railway project or the construction of a building near an existing line, a detailed design is required [23] possibly using comprehensive 3D models with high computational cost. These include Fiala et al. [24] who developed a comprehensive BEM-FEM model to calculate building vibration and indoor noise. Alternatively, Galvín et al. [25] presented a coupled train-track-soil-structure 3D BEM-FEM model formulated in the time domain where the nonlinear behaviour of structures could be also considered. Moreover, the problem of vibration in bridges was studied using comprehensive models as shown in [26,27]. Coulier et al. [28] studied the source (track) and receiver (building) interaction in order to determine the uncertainty of using uncoupled approaches. It was concluded that for a ballasted track the assumption of decoupling was acceptable for distances from the track greater than six times the Rayleigh wave length.

Uncoupled simplified procedures are normally used at early stages of railway line development [23]. These represent attractive tools due to their low computation times. Two such methods to evaluate building vibrations due to a train passage have been proposed by the Federal Railroad Administration (FRA) and the Federal Transit Administration (FTA) of the U.S. Department of Transportation [29–31]. Rücker et al. [32] developed a simplified prediction tool to evaluate free-field and building vibrations. Auersch [33] analysed building vibration in inhomogeneous soils and proposed a simplified methodology to consider SSI in layered ground. He studied building induced vibrations using a simple soil-wall-floor model based on an empirical transfer function obtained from the characteristics of the structure [34]. Moreover, this also included a simple method to estimate vibration in buildings on pile foundations [35]. Hussein et al. [36] developed a sub-modelling method where a train-track-soil 3D model was coupled with a 2D building approach based on beam elements. Hussein also presented a 3D model to calculate vibrations in a piled foundation building due to railway traffic from a nearby underground tunnel [37]. Later, Kouroussis et al. [38] proposed a decoupled FE model to predict building vibrations due to tramway traffic with local irregularities. Also a hybrid numerical/experimental model to assess ground and building vibration was presented [39,40]. In this a vehicle-track numerical approach which simulated vibration generation due to a variety of railroad artefacts was combined with a experimental procedure based on multiple single source transfer mobilities that modelled the transmission mechanism between rail and nearby structures. Lopes et al. [41,42] developed an uncoupled model to evaluate building vibrations induced by railway traffic in tunnels. Free-field response was computed using a 2.5 D FEM-Perfectly Matched Layers (PML) model and combined with a 3D FEM model to evaluate the building response. Connolly et al. [43,44] proposed a scoping model to predict vibrations and in-door noise in buildings due to railway traffic. A wide range of soil vibration records generated by a 3D FEM model was used to build a machine learning approach. This procedure was combined with empirical factors [31] to compute building vibrations. López-Mendoza et al. [45] presented a scoping model based on modal superposition analysis. The free-field vibration was discretised into the frequency range corresponding to the modes of the structure. Kuo et al. [46] presented a hybrid model that combined recorded data and numerical predictions considering the definitions proposed by the FRA [31]. The source, propagation and receiver mechanisms were uncoupled. Recently Connolly et al. [47] presented a decoupled procedure to analyse soil-building vibrations due to railway irregularities. A 2.5D time–frequency domain model to compute soil vibrations was combined with a 3D FEM procedure to obtain building vibrations induced by railway defects.

This paper uses a simple procedure where the source (ground motion) and the receiver (building) are uncoupled. It is focused on the receiver model and proposes soil-structure transfer functions considering SSI. These soil-structure transfer functions are combined with free-field vibrations to compute building vibration with low computational effort. The model is numerically verified by comparing with a comprehensive BEM-FEM model. Finally, the proposed model is used to analyse building vibrations due to railway local irregularities.

## 2. Methodology

ISO 14837-1 standard [23] defines the magnitude of building vibration $A(f)$ in the frequency domain $f$ as a function of the source $S(f)$, the propagation $P(f)$ and the receiver $R(f)$. Considering the assumption that all the three terms are uncoupled (Fig. 1), the magnitude of the building vibration $A(f)$ is expressed as:

$$A(f) = S(f)P(f)R(f) \tag{1}$$

The procedure developed by the Federal Railroad Administration (FRA) [31] to estimate building response due to railway traffic proposes two factors influencing the receiver: (1) the floor-to-floor attenuation, and, (2) the amplification due to the resonance of floors, walls and ceilings. The present work includes these factors defining the floor amplification $F_a$ as the increment in the building response $u$ with respect to the foundation response $u_0$ (Fig. 1). The floor amplification is computed as:

$$F_a(f) = u(f)/u_0(f) \tag{2}$$

Also, the effect of the building foundation should be considered using the coupling loss $C_l$ [31]. The coupling loss is related to the soil-foundation interaction. Therefore it is the ratio between the building foundation response $u_0$ and the free-field vibration $u_g$ (Fig. 1). In this work, the coupling is evaluated as:

$$C_l(f) = u_0(f)/u_g(f) \tag{3}$$

The following expression to calculate the building response $u$ can be obtained by combining Eqs. (2) and (3):

$$u(f) = F_a(f)C_l(f)u_g(f) \tag{4}$$

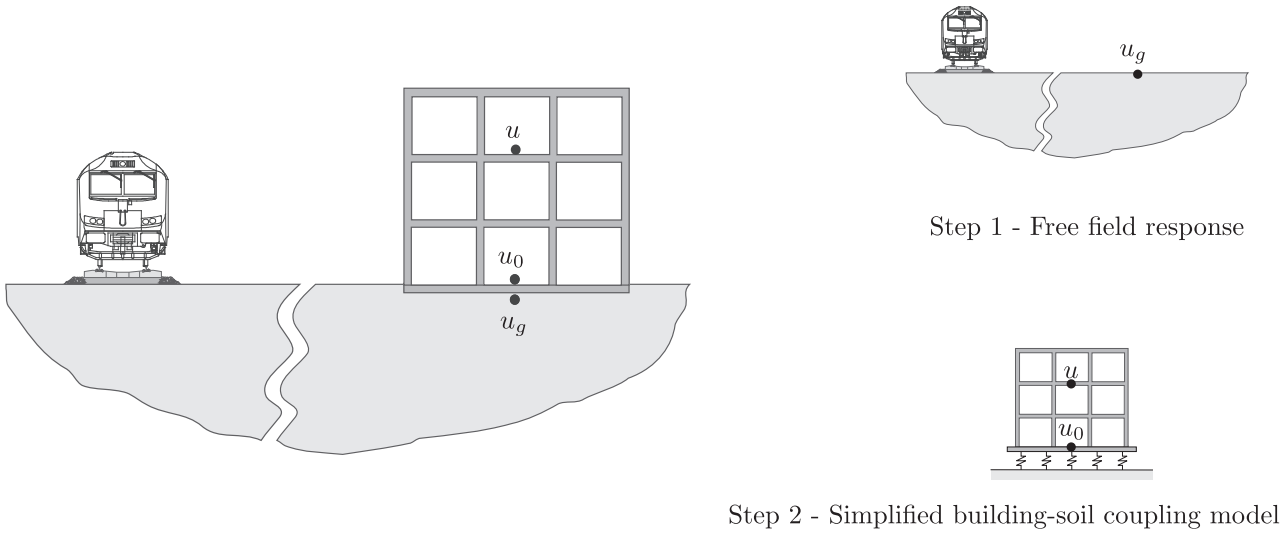


**Fig. 1.** (left) Coupled problem and (right) scheme of decoupled model.

Comparing Eqs. (1) and (4), it can be seen that the source $S(f)$ and the propagation $P(f)$ terms are included in the free-field vibration $u_g$, whereas the receiver term $R(f)$ is part of the floor amplification $F_a$ and the coupling loss $C_l$. In this approach, the problem is decoupled in two steps (Fig. 1): (i) computing or measuring the free-field vibration $u_g$ and (ii) the structural response induced by an incident wavefield considering a simplified building model. The main novelty of this work is applying the soil-structure transfer functions $u/u_g = F_a(f)C_l(f)$ depending only on the receiver, to predict building vibration by railway traffic. The soil-structure transfer function represents the building response due to a displacement impulse applied at the building foundation. A key advantage of this approach is the computational efficiency arising because the soil-structure transfer function is computed only once for a soil-building subsystem and later it is combined with a wide range of free-field vibration data to analyse multiple scenarios. These low requirements mean the approach is well-suited to early stage railway projects. On the other hand, although this work is focused on the application of soil-structure transfer functions to assess building vibrations by railway traffic, these soil-structure transfer functions can be used to predict building vibration due to diverse sources (e.g. construction, earthquake, road traffic, blast) where the free-field vibration spectrum is known.

### 2.1. Step 1 – Free field response

This work uses the methodology presented in Reference [47] to model the source-propagation subsystem $(S(f), P(f))$. It has been extended and validated, as discussed in [47], for the computation of free-field vibrations due to railway defects (Fig. 2), so is not repeated here. The free-field response is required as the input for Step 2, and can be either computed or measured using in situ tests. Once it is known for the source-propagation subsystem, it is used in Step 2 to compute the building vibration $A(f)$. To do so, the building foundation is excited by the free-field response $u_g(f)$. The SSI is integrated in the proposed methodology using a simplified method. Below, it will be related the procedure to model the receiver soil-structure subsystem $(R(f))$.

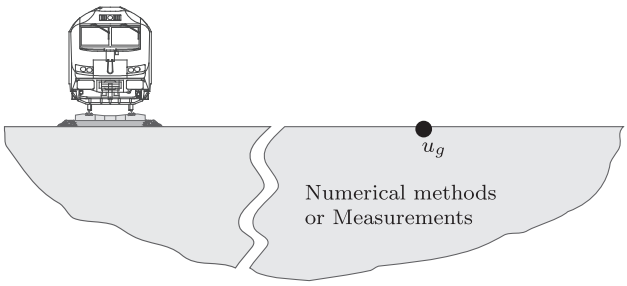


**Fig. 2.** Step 1 – Free field response.

### 2.2. Step 2 – Simplified building-soil coupling model

The simplified method is a 3D time domain FEM model. The dynamic equilibrium equation of a structure can be written as:

$$\mathbf{M}\ddot{\mathbf{u}}(t) + \mathbf{C}\dot{\mathbf{u}}(t) + \mathbf{K}\mathbf{u}(t) = \mathbf{F} \tag{5}$$

where $\mathbf{M}, \mathbf{C}$ and $\mathbf{K}$ are the mass, damping and stiffness matrices, respectively. $\mathbf{u}(t), \dot{\mathbf{u}}(t)$, and $\ddot{\mathbf{u}}(t)$ are the building displacement, velocity and acceleration, respectively, while $\mathbf{F}$ represents the external force. The FEM equation is solved at each time step following an implicit time integration GN22 Newmark method [48,49]. Structural damping is considered using a Rayleigh model [50], where the damping matrix $\mathbf{C}$ is proportional to the mass $\mathbf{M}$ and stiffness $\mathbf{K}$ matrices: $\mathbf{C} = d_m\mathbf{M} + d_k\mathbf{K}$. Constants $d_m$ and $d_k$ are chosen depending on the modal damping of the structure.

The simplified method is based on recommendations from the National Institute of Standards and Technology (NIST) [51]. This proposes to integrate SSI by adding spring-damper elements to the foundation of the building. As the building is not embedded in the soil, expressions to define horizontal spring-damper elements are discarded. The formulation to calculate vertical spring-damper elements is below.

To explain the simplified model, consider a rectangular building with floor plan dimensions $2L \times 2B$, where $L \geqslant B$ (Fig. 3). Note that in the following formulation, the sub-indices $x, y$ and $z$ are related to the translation along the respective axis. Also the sub-indices $xx$ and $yy$ refer the rocking about the $x$ and $y$ respectively, whereas sub-index $zz$ is related to the torsion about the $z$ axis (Fig. 3). Hereafter, the formulation considers the $x$ axis to be the largest dimension of the foundation ($2L$).

A spring-damper system is added to the foundation allowing it to be modelled as rigid or flexible. For the rigid case, a single spring-damper element defined by its stiffness $k_z$ and the dashpot coefficient $c_z$. On the other hand, flexible foundations are simulated

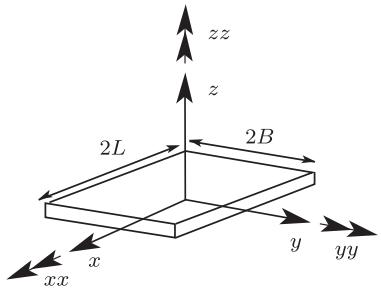


**Fig. 3.** Scheme of the plan geometry of the building foundation.

using spring-damper elements ($k_z^i$, $c_z^i$) spread across the foundation area, where $k_z^i$ and $c_z^i$ are the properties of the $i^{th}$ spring-damper element.

*2.2.1. Rigid foundation*

If the foundation is rigid, it can be represented by a single spring-damper element ($k_z$, $c_z$). The vertical stiffness of the full system $k_z$, is evaluated using the formulation presented in Reference [52]:

$$k_z = K_{z,surf}\alpha_z \tag{6}$$

where $K_{z,surf}$ is the vertical static stiffness of the surface foundation and $\alpha_z$ is the dynamic stiffness modifier. The vertical static stiffness $K_{z,surf}$ is obtained from the shear modulus $G$ and Poison's ratio of the soil $\nu$, and the foundation dimensions $L$ and $B$, using:

$$K_{z,surf} = \frac{GB}{1-\nu}\left(3.1\left(\frac{L}{B}\right)^{0.75} + 1.6\right) \tag{7}$$

Also the dynamic stiffness modifier $\alpha_z$ depends on the structural properties and is evaluated as:

$$\alpha_z = 1 - \frac{\left(0.4 + \frac{0.2}{\frac{L}{B}}\right)a_0^2}{\frac{10}{1+3\left(\frac{L}{B}-1\right)} + a_0^2} \tag{8}$$

where $a_0$ is the dimensionless frequency computed from the S-wave velocity $c_s$ and the angular frequency of the first bending mode $\omega_1$ (discarding SSI), as:

$$a_0 = \frac{\omega_1 B}{c_s} \tag{9}$$

Once the vertical stiffness $k_z$ is obtained, the dashpot coefficient of the full foundation $c_z$ can be computed using [51]:

$$c_z = 2k_z\frac{\beta_z + \beta_s}{\omega_1} \tag{10}$$

where $\beta_s$ is the damping ratio of the soil and $\beta_z$ is the radiation damping ratio obtained as [52]:

$$\beta_z = \frac{4\psi\frac{L}{B}}{\frac{K_{z,surf}}{GB}}\frac{a_0}{2\alpha_z} \tag{11}$$

where $\psi = \sqrt{2(1-\nu)(1-2\nu)}$, limited to $\psi \le 2.5$. Following the same procedure to calculate the vertical stiffness $k_z$ (Eq. (6)), the rocking stiffness can be obtained as [52]:

$$k_{yy} = K_{yy,surf}\alpha_{yy}k_{xx} = K_{xx,surf}\alpha_{xx} \tag{12}$$

The rocking static stiffnesses ($K_{xx,surf}, K_{yy,surf}$) and the dynamic stiffness modifiers ($\alpha_{xx}, \alpha_{yy}$) are evaluated as:

$$K_{yy,surf} = \frac{GB^3}{1-\nu}\left(3.73\left(\frac{L}{B}\right)^{2.4} + 0.27\right)$$
$$K_{xx,surf} = \frac{GB^3}{1-\nu}\left(3.2\left(\frac{L}{B}\right) + 0.8\right) \tag{13}$$

$$\alpha_{yy} = 1 - \frac{0.55a_0^2}{0.6 + \frac{1.4}{\left(\frac{L}{B}\right)^3} + a_0^2}$$
$$\alpha_{xx} = 1 - \frac{\left(0.55 + 0.01\sqrt{\frac{L}{B}-1}\right)a_0^2}{2.4 - \frac{0.4}{\left(\frac{L}{B}\right)^3} + a_0^2} \tag{14}$$

In the same way as for the vertical dashpot (Eq. (10)), the rocking dashpot is computed as [52]:

$$c_{yy} = 2k_{yy}\frac{\beta_{yy} + \beta_s}{\omega_1}$$
$$c_{xx} = 2k_{xx}\frac{\beta_{xx} + \beta_s}{\omega_1} \tag{15}$$

where the radiation damping ratios $\beta_{xx}$ and $\beta_{yy}$ are calculated as:

$$\beta_{yy} = \frac{\frac{4\psi}{3}\left(\frac{L}{B}\right)^3 a_0^2}{\frac{K_{yy,surf}}{GB^3}\left(\frac{1.8}{1+1.75\left(\frac{L}{B}-1\right)} + a_0^2\right)}\frac{a_0}{2\alpha_{xx}}$$
$$\beta_{xx} = \frac{\frac{4\psi}{3}\frac{L}{B}a_0^2}{\frac{K_{xx,surf}}{GB^3}\left(2.2 - \frac{0.4}{\left(\frac{L}{B}\right)^3} + a_0^2\right)}\frac{a_0}{2\alpha_{yy}} \tag{16}$$

*2.2.2. Flexible foundation*

Eqs. (6) and (10) compute the spring-damper element ($k_z, c_z$) properties for rigid foundations. However, in order to consider the effect of a flexible foundation, the NIST proposes smeared spring and damper elements. To do so, the vertical values $k_z$ and $c_z$ are normalized by the foundation area to obtain the stiffness intensity $\tilde{k}_z^i = k_z/4BL$ and dashpot intensity $\tilde{c}_z^i = c_z/4BL$. Then, the stiffness $k_z^i$ and dashpot $c_z^i$ of a vertical spring-damper element in the interior of the foundation can be computed as:

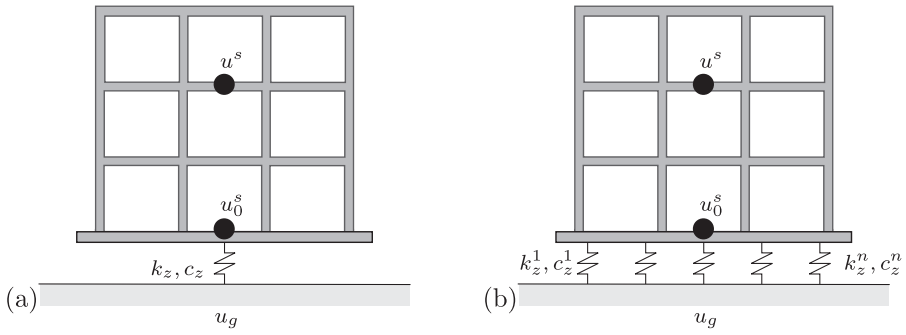


**Fig. 4.** Step 2 – Simplified building-soil coupling model: (a) rigid foundation and (b) flexible foundation.

$$k_z^i = \tilde{k}_z^i dA^i \quad c_z^i = \tilde{c}_z^i dA^i \tag{17}$$

where $dA^i$ is the individual area for the $i^{th}$ spring-damper element (Fig. 5). If these expressions (Eq. (17)) are used across the full foundation, the rotational stiffness would be underestimated and the rotational damping would be overestimated [51]. To correct these effects, factors $R_k$ and $R_c$ are applied to the spring-damper elements along a strip area on the foundation edge. To do so, the stiffness and damping of a vertical spring-damper element at the foundation edge are estimated as:

$$k_z^i = R_k \tilde{k}_z^i dA^i \quad c_z^i = R_c \tilde{c}_z^i dA^i \tag{18}$$

The width of the foundation edge strip is computed from the foundation end ratio $R_e$ as $R_eL$ and $R_eB$ for the $x$ and $y$ axes, respectively. A value in the range from 0.3 to 0.5 is usually selected for the foundation end ratio $R_e$. In this work an end ratio $R_e = 0.5$ is used. Fig. 6 shows the spring-damper element properties $(k_z^i, c_z^i)$ depending on the position of the $i^{th}$ element across the foundation.

Regarding the estimation of the correction factors $R_k$ and $R_c$, the following expressions are proposed by NIST:

$$R_{k,yy} = \frac{\frac{3k_{yy}}{4\tilde{k}_z^i BL^3} - (1-R_e)^3}{1-(1-R_e)^3}$$
$$R_{k,xx} = \frac{\frac{3k_{xx}}{4\tilde{k}_z^i B^3 L} - (1-R_e)^3}{1-(1-R_e)^3} \tag{19}$$

$$R_{c,yy} = \frac{\frac{3c_{yy}}{4\tilde{c}_z^i BL^3}}{R_{k,yy}\left(1-(1-R_e)^3\right) + (1-R_e)^3}$$
$$R_{c,xx} = \frac{\frac{3c_{xx}}{4\tilde{c}_z^i BL^3}}{R_{k,xx}\left(1-(1-R_e)^3\right) + (1-R_e)^3} \tag{20}$$

where $k_{xx}$ and $k_{yy}$ are the rotational stiffnesses about the $x$ and $y$ axes respectively, considering a rigid foundation. Also the dashpot coefficients $c_{xx}$ and $c_{yy}$ represent the rotational damping about the $x$ and $y$ axes respectively.

### 2.3. Accounting for soil layering

In order to consider SSI for layered soils, equivalent homogeneous soils are obtained depending on the average shear wave velocity $V_{s30}$ as defined in Eurocode 8 [53], and computed as:

$$V_{s30} = \frac{30\,[\mathrm{m}]}{\sum_i^{N_s} \frac{h_i}{c_{s_i}}} \tag{21}$$

where $h_i$ is the thickness of the $i$th layer, $N_s$ the total number of layers in the top 30 m and $c_{s_i}$ the shear wave velocity of the $i$th layer. Therefore, equivalent homogeneous soils with $c_s = V_{s30}$ are considered to model layered soils. $V_{s30}$ is a measure of the mean shear wave speed in the top 30 m of soil [53]. Free-field vibrations can be satisfactorily obtained from this simplification for soil profiles with smooth stratigraphy's [54]. However, the building response, once $u_g(f)$ is computed or measured, is not significantly influenced by soil stratification [55,56].

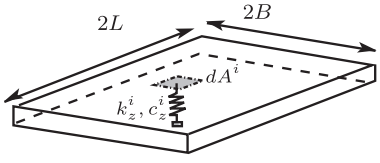


**Fig. 5.** Individual area $dA^i$ for the $i$ spring-damper element.

### 2.4. Methodology summary

The methodology for calculating building response, including SSI is as follows:

1. The free-field vibration field is computed or measured in situ (i.e. the ground surface response due to train passage).
2. The spring-damper system supporting the building foundation is computed using soil properties $(c_s, G, \nu, \beta_s)$, foundation geometry $(B, L)$ and first bending mode $(\omega_1)$.
3. These inputs are used to obtain the spring-damper system properties for either a rigid foundation (Eqs. (6) and (10)) or a flexible foundation (Eqs. (17) and (18)).
4. The spring-damper system is assembled/combined with the building model. This allows for the construction of the global mass, damping and stiffness matrices $(\mathbf{M}, \mathbf{C}, \mathbf{K})$.
5. The soil-structure transfer function $u/u_g = F_a(f)C_l(f)$ is computed by solving the dynamic equilibrium equation of the structure due to a displacement impulse applied at its foundation (Eq. (5)). (Note however that, $F_a(f)$ and $C_l(f)$ factors can be independently computed as it is done in the next section.)
6. The soil-structure transfer function is combined with the free-field vibration $u_g$ [47] to obtain the building response $u$ due to an arbitrary excitation (Eq. (4)). Using a logarithmic scale, the coupling loss and the floor amplification are added to the free-field response.

## 3. Building-soil model approach

In this section, the dynamic behaviour of three buildings are compared with those obtained from the `SSIFiBo` toolbox [57]. The `SSIFiBo` toolbox represents a comprehensive model based on a 3D time domain BEM-FEM methodology. The solution $u^r$ represents the building response from `SSIFiBo` toolbox, hereafter called the 'reference' solution, whereas $u^s$ is the solution computed using the simplified method considering flexible foundation. A third solution is also computed for each case, where SSI $\tilde{u}$ is ignored.

The following analysis compares the numerical results using the methodologies depicted in Figs. 4 and 7: (i) a 'reference model', consisting of a FEM building model coupled with a BEM soil model, (ii) a FEM building model with SSI ignored, and (iii) the proposed simplified methodology accounting for SSI.

To quantify the effect of SSI, it is studied using the ratio:

$$\Delta u^s(f) = \frac{u^s(f)}{\tilde{u}(f)} \tag{22}$$

Substituting Eq. (4) into Eq. (22) and remembering that the coupling loss $\tilde{C}_l$ for the solution without SSI is equal to 1, the SSI effect can be rewritten as:

$$\Delta u^s = C_l^s F_a^s / \tilde{F}_a \tag{23}$$

This work uses the assumption that SSI depends only on the coupling loss $\Delta u^s \approx C_l^s$. Substituting this simplification in Eq. (23) means that the solution ignoring SSI presents floor amplifications close to those obtained using the simplified method $F_a^s/\tilde{F}_a \approx 1$. This simplification is advantageous in practice because it allows for the computation of $F_a$ using building models where the soil is neglected. Then, the effect of SSI can be considered by adding the coupling loss $C_l$ to the transfer function $F_a$, which has been made available for common buildings in standards [29–31].

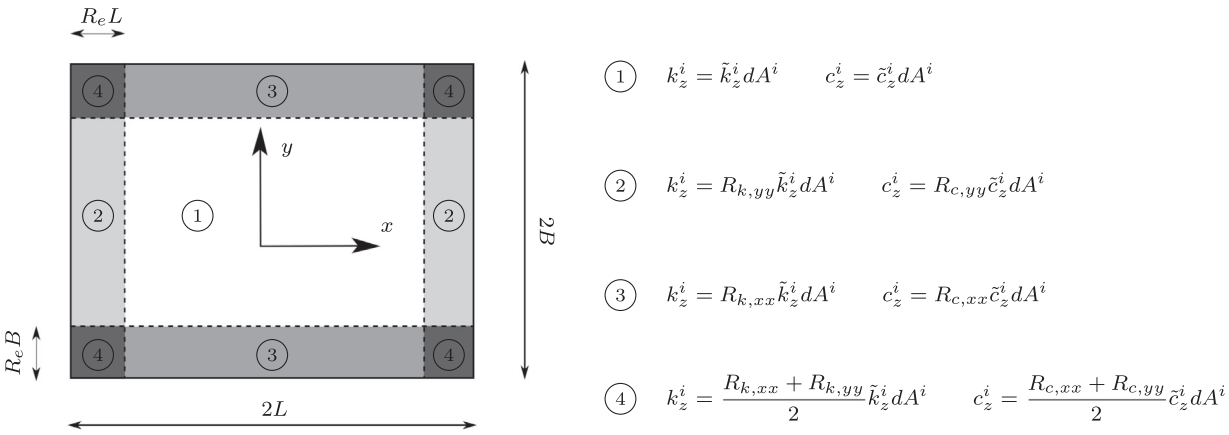


**Fig. 6.** Spring-damper element properties across the foundation.

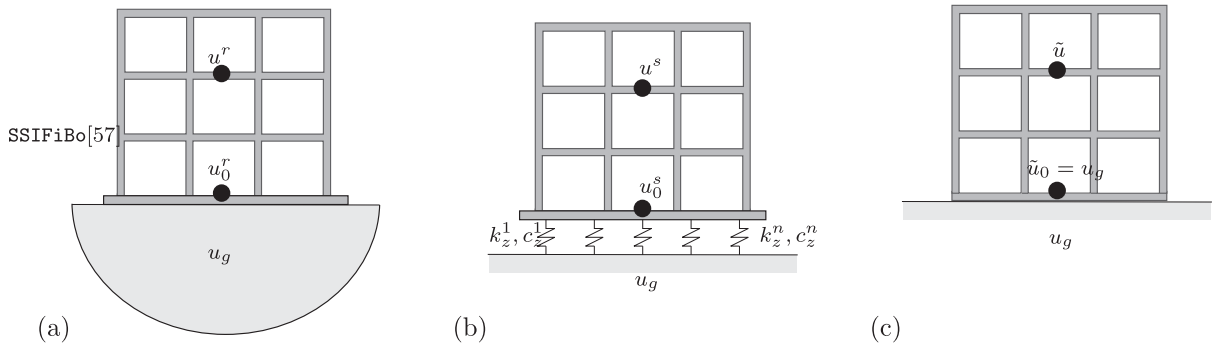


**Fig. 7.** (a) 'Reference' model with soil explicitly modelled, (b) proposed decoupled model and (c) model with SSI ignored.

### 3.1. Building response induced by an incident wavefield

The analysis of buildings excited due to an incident wavefield allows for the computation of the coupling loss $C_l$ and the floor amplification $F_a$ factors needed to obtain the building response due to an arbitrary load. Moreover, this analysis allows for the evaluation of the accuracy of the simplified method (Section 2.2) and the coupling loss assumption described above.

The three types of building consist of four, six and twelve storey concrete buildings founded on a slab, with framed walls (Fig. 8). Floor plan dimensions of $12\,\text{m} \times 40\,\text{m}$, $20\,\text{m} \times 20\,\text{m}$ and $12\,\text{m} \times 12\,\text{m}$ are considered for the four, six and twelve storey buildings, respectively. The floors are simply supported concrete slabs. Four edge beams are considered in the twelve storey building. The concrete material has the following properties: Young's modulus $E = 20 \times 10^9\,\text{N/m}^2$, Poisson's ratio $\nu = 0.2$ and density $\rho = 2400\,\text{kg/m}^3$. A structural damping, $\zeta = 5\,\%$ is set for the dominant mode shapes (Fig. 9). The structures are discretised using two-node Euler-Bernoulli elements to represent columns and beams and four-node shell elements for the floors and the framed walls. The finite element representation is determined by the discretization of the structure with respect to bending wavelength. The minimum wavelength is defined by the maximum frequency range and the phase bending wave propagation speed $c_B = \sqrt[4]{\omega_1^2 EI_z/m_b}$, where $EI_z$ is the beam cross-section bending stiffness, $m_b$ is the beam mass per unit length and $\omega_1$ corresponds to the fundamental frequency of the structure. 20 elements per minimum wavelength were used for all analysis in this work. Table 1 summarises the building properties.

The dominant bending mode shapes computed without considering SSI can be observed in Fig. 9. The vertical bending mode shapes depend mainly on the floor spans and structural typology. Here, two structural typologies have been analysed, with the 12-storey building being stiffer than the others due to the concrete walls located at its center.

The buildings are on a homogeneous soil with P-wave velocity $c_p = 250\,\text{m/s}$, S-wave velocity $c_s = 100\,\text{m/s}$, material damping $\xi = 0.06$ and density $\rho = 1750\,\text{kg/m}^3$. The building responses are presented for the observation points $A$ and $B$ (Fig. 8). The incident wave field consists of a uniform vertical displacement $\tilde{\mathbf{u}}_g = \delta(t)\,\text{m}$, where $\delta$ is the Dirac delta function. Therefore, the incident wave field in the frequency domain presents a constant value. This incident wave field allows for the calculation of the building response solely in terms of the receiver $u(f) = F_a(f)C_l(f)$ (Eq. (4)). Also the coupling loss represents the foundation response $C_l(f) = u_0(f)$ (Eq. (3)).

Fig. 10 shows the one-third octave band representation of the coupling loss computed using the reference model and the simplified method. It was computed according to the German standard DIN 45672-2 [58], considering a reference period during which the response was considered to be stationary. This representation allows for the evaluation of human exposure to whole-body vibration according to the k-curves defined in Reference [59] or using the methodology proposed in References [29–31].

Generally, at frequencies higher than the fundamental bending mode shape of the building, the coupling loss factor is negative. This means that the SSI attenuates the structural response, and $C_l(f)$ reaches maximum values at the natural frequencies of the soil-foundation system. The coupling loss factor varies over a

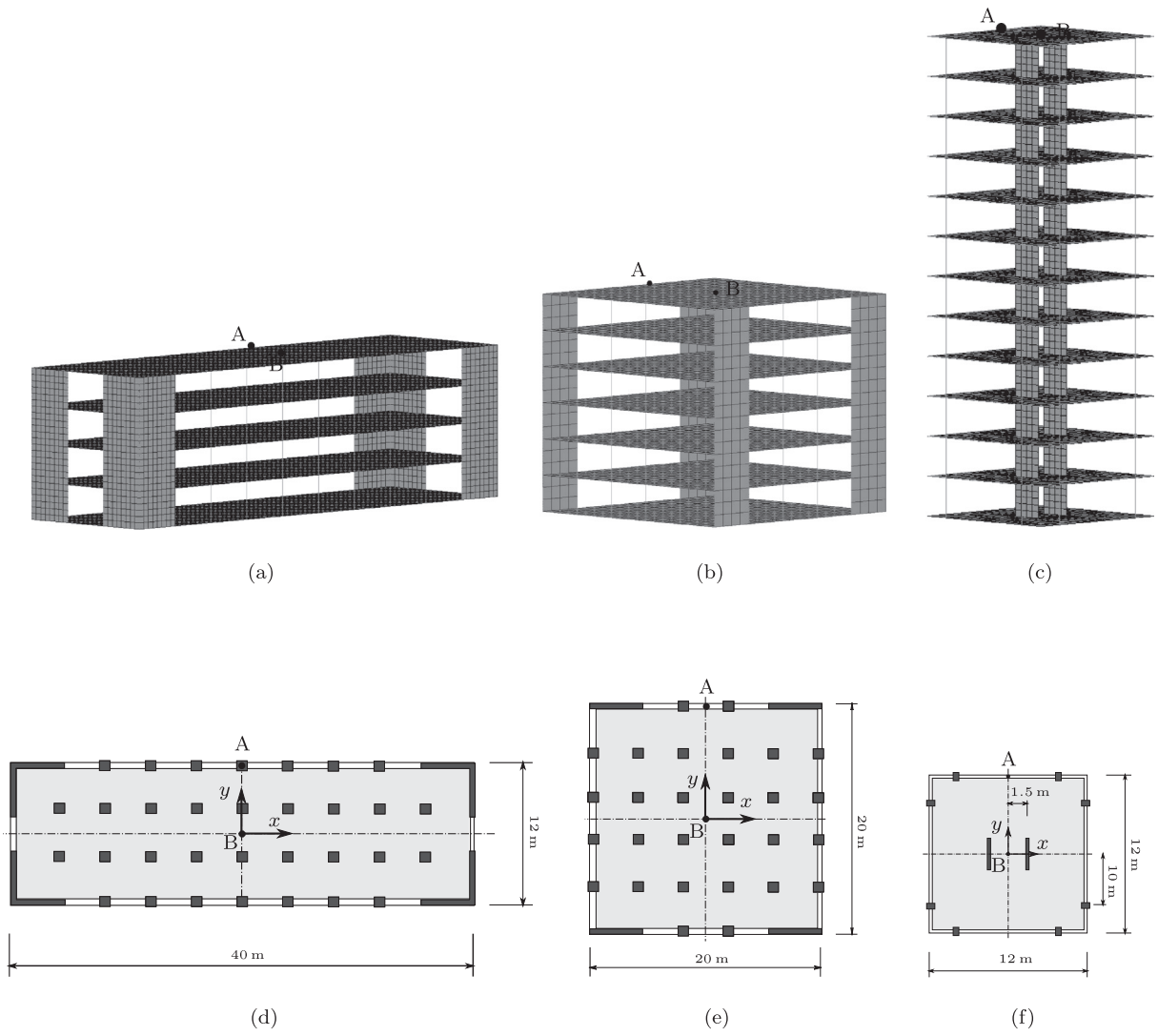


**Fig. 8.** Discretization and plan geometry of the (a, d) four, (b, e) six and (c, f) twelve-storey buildings.

10 dB range and depends on the type of building and the observation point. References [29–31] provide a constant value for all frequencies, ranging from −13 dB (large masonry on spread footings) to 0 dB (foundation in rock) depending on the type of building. A frequency dependent coupling factor predominantly less than −13 dB is obtained using the simplified model, and is consistent with that expected for this type of building (≈ −10 dB). Further, the 'reference' model produces even lower attenuation, showing that the values given in standards should be used with caution.

The vibration at the center of the foundation is lower than that at the side of the building closest to the excitation, in the low frequency range. However, at higher frequencies, the center of the foundation presents the highest level according to mode shape deformation. It should be noted that the simplified model is composed of spring-damper elements which have modified properties depending upon location (Fig. 6). Nevertheless, the spring-dampers at the center of the foundation are unmodified and thus the stiffness and damping values are not overestimated.

The comparison between the results computed from both methodologies shows that the simplified methodology yields higher attenuation factors compared to the 'reference' model. This is because the simplified approach models the soil-flexible foundation system using a set of spring-damper elements, meaning it has softer properties than the actual soil. Finally, it should be noted that References [29–31] show that heavier buildings result in greater coupling loss. The proposed model is consistent with this finding.

The floor amplification (Eq. ( 2)) is shown in Fig. 11 from the first to fourth floors, for the simplified and reference models, and the case of ignoring SSI. Overall the floor amplification increases with storey level in the low frequency range, while the excitation is filtered at higher frequencies according to the modal parameters of the buildings. The floor amplification yields maximum values at the floor local resonance frequencies. At frequencies higher than the fundamental bending mode shapes of the floors, the floor amplifications have negative values.

Regarding the 'reference' model, the simplified methodology underestimates the floor amplification at higher frequencies, while the solution ignoring SSI overestimates the response. According to References [29–31], the amplification due to the resonances of floors is +6 dB, but lower near the wall-floor and wall-ceilings intersections. In the present analysis, the maximum value obtained is 10.5 dB from the simplified model and 9.2 dB from the 'reference' model. The model ignoring SSI provides the highest floor amplification.

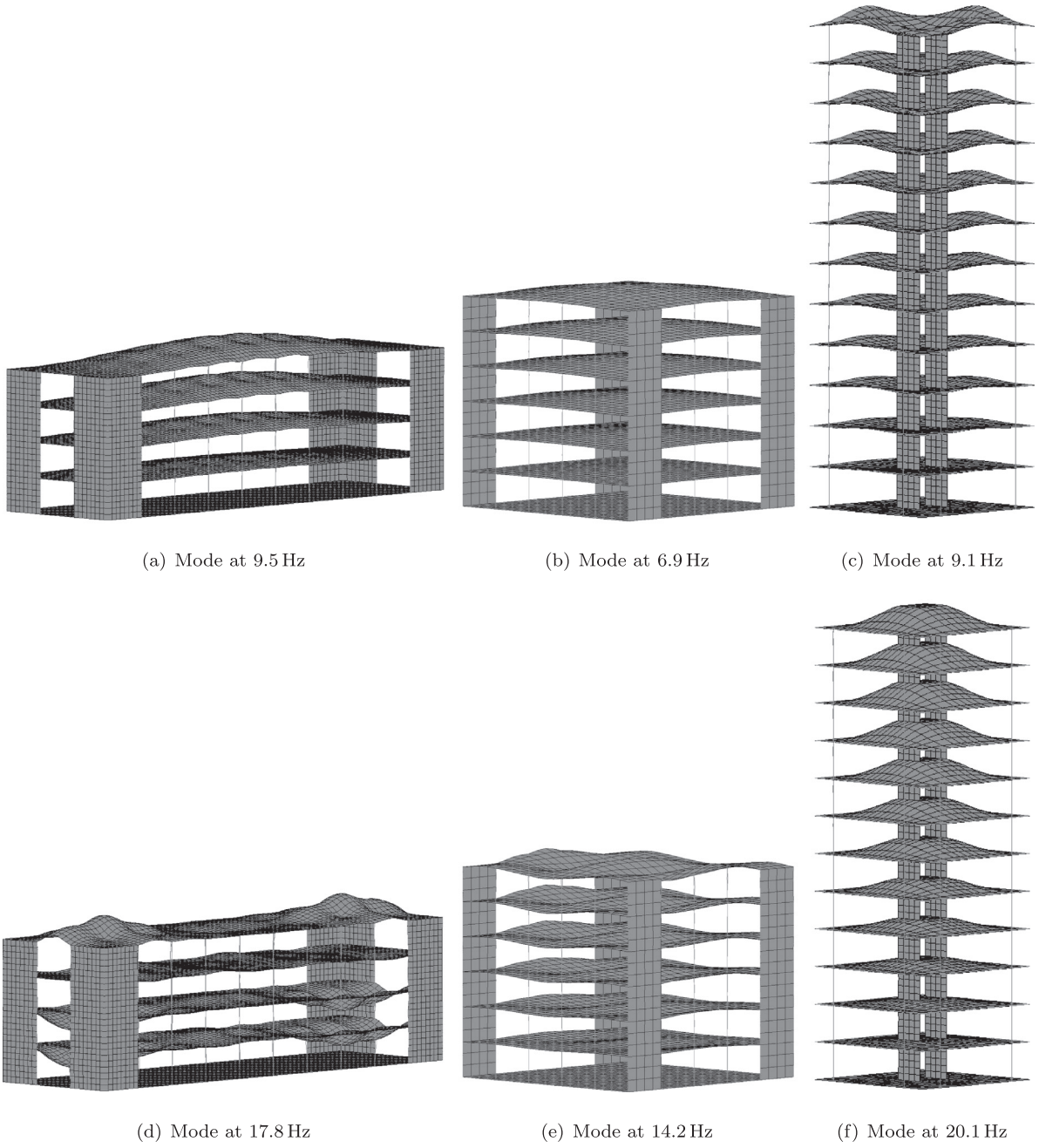

(a) Mode at 9.5 Hz (b) Mode at 6.9 Hz (c) Mode at 9.1 Hz

(d) Mode at 17.8 Hz (e) Mode at 14.2 Hz (f) Mode at 20.1 Hz

**Fig. 9.** Dominant bending mode shapes of the (a,d) four-storey building, (b,e) and (c,f) twelve-storey building.

**Table 1**
Building properties.

| | 4-storey | 6-storey | 12-storey |
|---|---|---|---|
| Column section $[m^2]$ | $0.3 \times 0.3$ | $0.3 \times 0.3$ | $0.6 \times 0.4$ |
| Edge beam section $[m^2]$ | – | – | $0.6 \times 0.2$ |
| Frame wall thickness [m] | 0.25 | 0.25 | 0.15 |
| Floor slab thickness [m] | 0.25 | 0.25 | 0.2 |
| Foundation slab thickness [m] | 0.5 | 1 | 1 |

Fig. 12 presents the soil-structure transfer function $u(f)/u_g(f)$ for all 3 models. This soil-structure transfer function is obtained from the receivers terms $u(f)/u_g(f) = F_a(f)C_l(f)$ (Eq. (4)) and relates the structural response to the load. It can be concluded that the shape and magnitude of the response from the simplified method match reasonable well with those obtained from the 'reference' model, although the results from the simplified method are underestimated. This is due to the high attenuation of the ground-building coupling shown in Fig. 10. Therefore the response ignoring SSI overestimates the results at frequencies higher than the floor resonance.

The global effect of SSI on the building response is shown in Fig. 13, which displays the ratio $\Delta u^s$ (Eq. (22)) for all building floors. These ratios represent the changes in the building response due to SSI, computed using the proposed methodologies. Also, it superimposes the coupling loss factor $C_l^s$ to evaluate the accuracy of the approximation $\Delta u^s \approx C_l^s$, defined above. Although there are amplifications at low frequencies, particularly at the floors closest to the ground, it can be seen that there are attenuations in the mid and high frequency ranges due to SSI. It is observed that the effect of

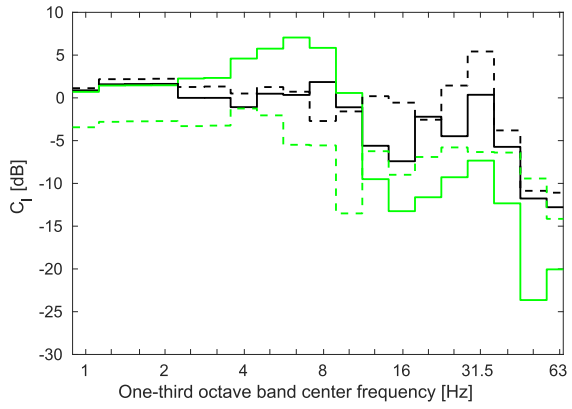


(a)

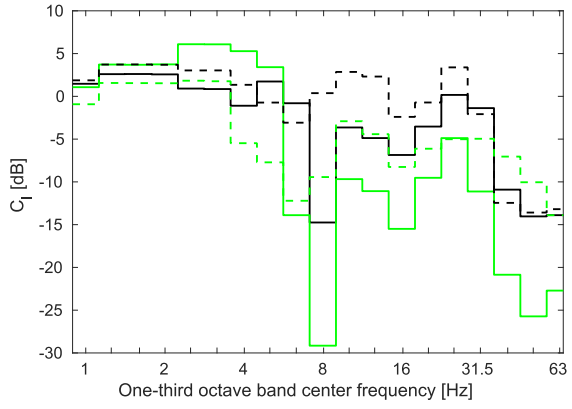


(b)

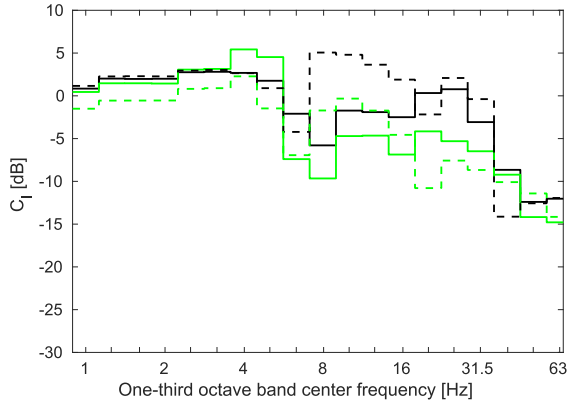


(c)

**Fig. 10.** One-third octave band center frequency of the coupling loss due to an incident wave field, at the projection of the observation points (solid line) *A* and (dashed line) *B* on the foundation of the (a) four-storey, (b) six-storey and (c) twelve-storey buildings, from the (black line) `SSIFiBo` toolbox and the (green line) simplified methodology. (For interpretation of the references to colour in this figure legend, the reader is referred to the web version of this article.)

SSI is weakly dependent on storey level, with the greatest effect evident on the tallest building. This analysis leads to the possibility of studying of the structural response using a building model where the soil is not considered, and modelling SSI as an attenuation of the computed response, as suggested in some standards. This attenuation can be estimated using the coupling loss factor obtained from the proposed methodology because it represents an approximate envelope as shown in Fig. 13.

## 4. Case study: railway track defects

The proposed methodology is now used to analyse building vibration due to local track defects. The building response is calculated by combining the free-field $u_g$ response due to railway traffic (Fig. 2) with the soil-structure transfer function $u(f)/u_g(f) = F_a(f)C_l(f)$ (Eq. (4)) due to an incident wave field computed in the previous section using the simplified model shown in Fig. 4. The free-field response is calculated using a methodology experimentally validated in Reference [47]. Therefore this paper aims to use these excitation time histories as example datasets, rather than to validate or address the assumptions associated with the underlying excitation generation model. Moreover, it is focused on the effect of local track defects on the response of building using the proposed numerical method, rather than the analysis of track forces due to defects.

Using a pre-determined excitation facilitates reduced computational effort because the soil-structure transfer function $u(f)/u_g(f)$ does not depend on train passage and is thus only evaluated once. Therefore, the proposed methodology presents a major computational advantage compared to existing numerical procedures where the track-soil-building system is recomputed every time the train passage changes. The proposed approach is thus similar to the FTA standard: the soil-building system is modelled using coupling loss and floor amplification factors (step 2), while the excitation is measured or computed (step 1). Once $u_g(f), C_l(f)$ and $F_a(f)$ are obtained, the structural response is computed with minimal effort using multiplication (linear scale) or addition (logarithm scale).

A sensitivity analysis of the effect of defect type and size is presented. Fig. 14 shows the singular defects considered in the analysis, where $v_0$ is the train speed, $h$ the defect height and $l$ the defect length. The defect size influence on building vibrations is analysed considering several defect lengths $l = \{80, 110, 140, 170, 200\}$ mm.

Vibrations are obtained for the six storey building analysed previously in Section 3 (Fig. 8). The midpoint of the building foundation is located at a distance, $d = 30$ m, from the track centreline and observation point *B* (Fig. 8) is selected because it presents the highest response. Also, building vibrations are calculated considering a single point response (SPR) excitation model, where the free-field vibration is transmitted simultaneously to the whole building foundation. The SPR model is used for obtaining the maximum response level threshold, accounting for the minimum distance from the building foundation to the track (i.e. 20 m). Alternatively, changing the implementation to a multiple point response (MPR) excitation model would also be straightforward but is not considered here. The soil was considered as a homogeneous half-space with: $E = 100$ MPa, $\nu = 0.35, \zeta = 0.05$, and $\rho = 2000$ kg/m$^3$. The shear wave velocity was $V_s = 136.1$ m/s.

Two vehicle configurations were analyse: (i) an AM96 intercity train (Fig. 15) travelling on a ballasted track (Table 3), and (ii) a classic tram (Fig. 16) on an urban slab track (Table 4). The vehicles were modelled using a detailed multibody vehicle approach [60]. The AM96 and classic tram properties are shown in Table 2.

Fig. 17. (a) shows the free-field acceleration $a_g$ considering the passage of the AM96 train at $v_0 = 120$ km/h, over a ballasted track, in the presence of a negative pulse defect. Dominant frequencies are located at mid frequencies due to dynamic excitation. Also, the soil-structure transfer function $a/a_g$ in the frequency domain is shown for the building in Fig. 17. (b). The soil-structure transfer function shows amplifications at low and mid frequencies up to 30 Hz, whereas the response is damped at high frequencies. These

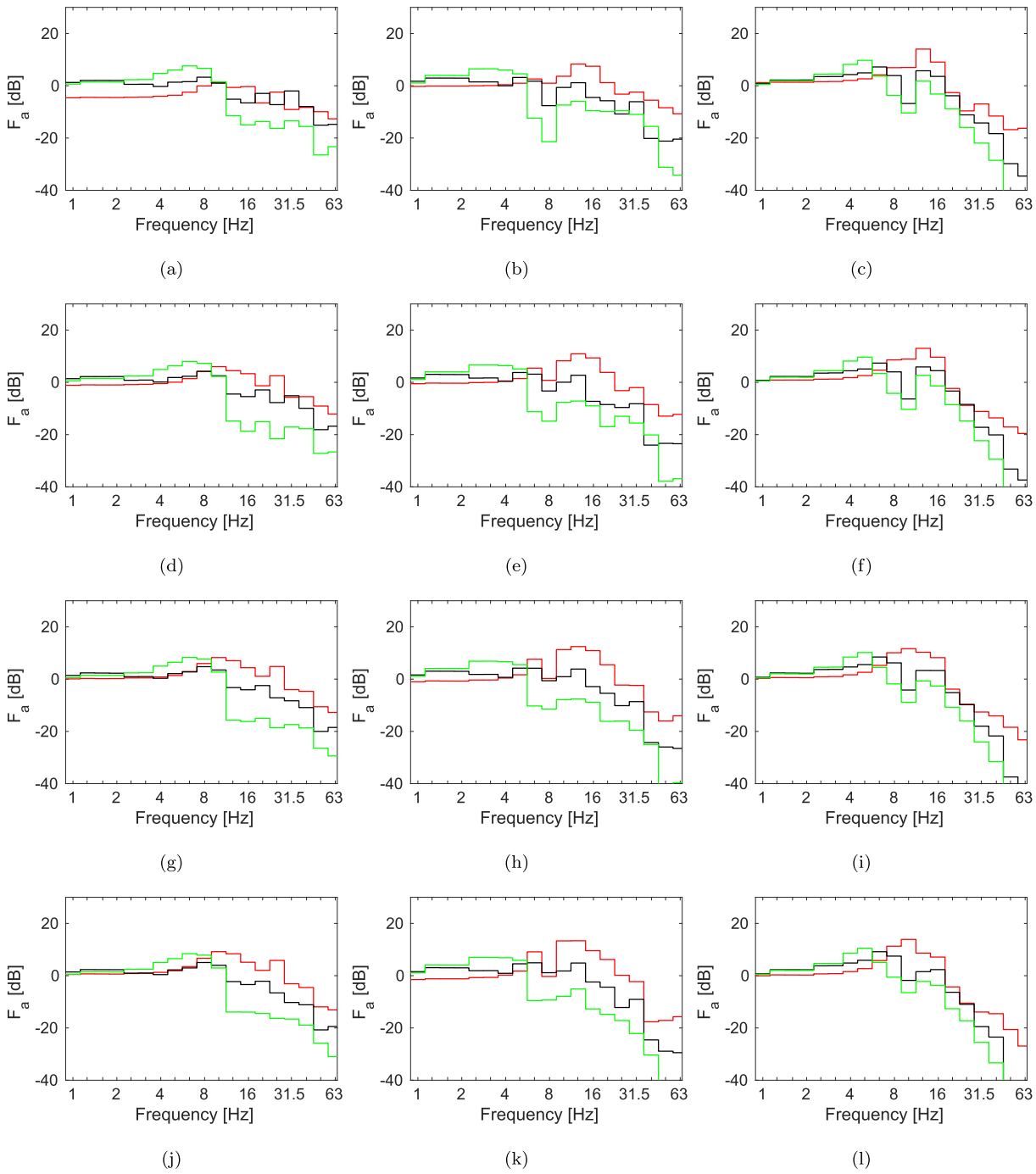


**Fig. 11.** One-third octave band center frequency of the floor amplification due to an incident wave field, at the observation point *A* of the (a,d,g,j) four-storey, (b,e,h,k,) six-storey and (c,f,i,l) twelve-storey buildings, at the (a,b,c) first, (d,e,f) second, (g,h,i) third and (j,k,l) fourth floors, from the (black line) `SSIFiBo` toolbox, the (green line) simplified methodology and (red line) ignoring SSI. (For interpretation of the references to colour in this figure legend, the reader is referred to the web version of this article.)

amplifications are concentrated at 20 Hz, corresponding to the natural frequencies of the building (Fig. 9) and, therefore, where the function $u/u_g = C_l(f)F_a(f)$ presents maximum values. Moreover, this frequency range matches with a maximum in the excitation.

Building vibration is obtained by combining the free-field response $a_g$ and the soil-structure transfer function (Fig. 17). Fig. 18 shows the frequency content[58] and the running RMS value of the building response. The running RMS value is computed using a time window of 1 s as prescribed by ISO 2631 [21]. In addition to the dominant frequencies indicated above, in the soil-structure transfer function $a/a_g$ (Fig. 17. (b)), the additional frequencies due to the source are significant. As previously mentioned, the proposed methodology is straightforward and it allows for the computation of the building response by summing the results shown in Fig. 17. The structural response in the low frequency range is amplified in relation to the source due to resonances at the dominant natural frequencies of the building. However, in the high frequency range, the excitation is attenuated according to the transfer function (shown in Fig. 17. (b)).

The results of the test case yield running RMS values lower than the threshold for harmful effects to humans according to ISO 2631 [21]. As an example, the Spanish standard [61] uses a maximum

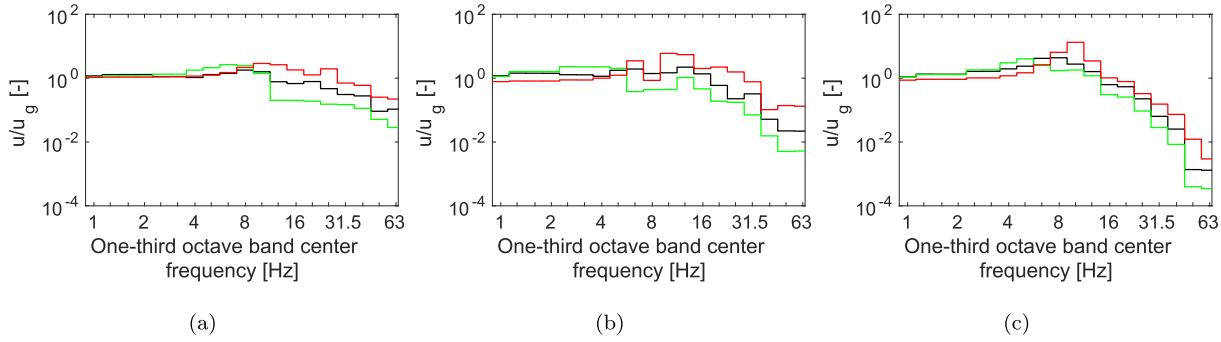


**Fig. 12.** One-third octave band center frequency of the soil-structure transfer function due to an incident wave field, at the observation point *A* of the (a) four-storey, (b) six-storey and (c) twelve-storey buildings, at the top floor, from the (black line) `SSIFiBo` toolbox, the (green line) simplified methodology and (red line) ignoring SSI. (For interpretation of the references to colour in this figure legend, the reader is referred to the web version of this article.)

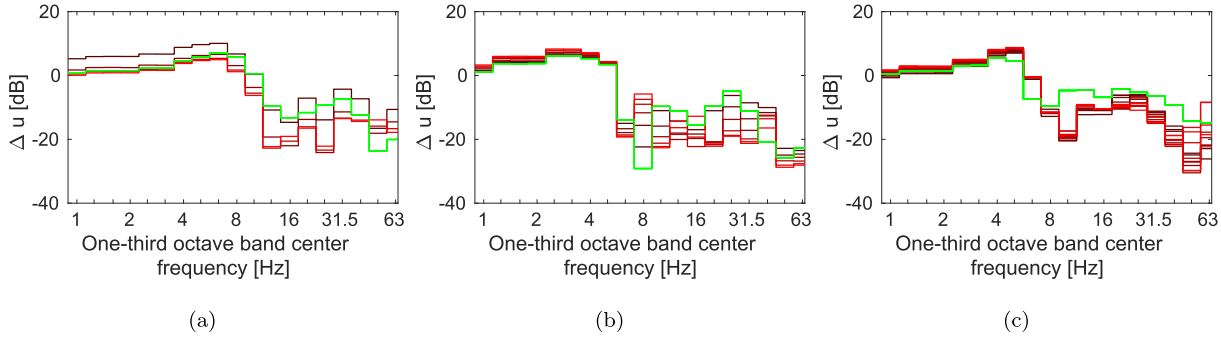


**Fig. 13.** One-third octave band center frequency of the ratio $\Delta u^s$ at the observation point *A* of the (a) four-storey, (b) six-storey and (c) twelve-storey buildings. SSI attenuation from the (darkest line) first floor to the (red line) top floor. Superimposed is the (green line) coupling loss computed from the simplified method. (For interpretation of the references to colour in this figure legend, the reader is referred to the web version of this article.)

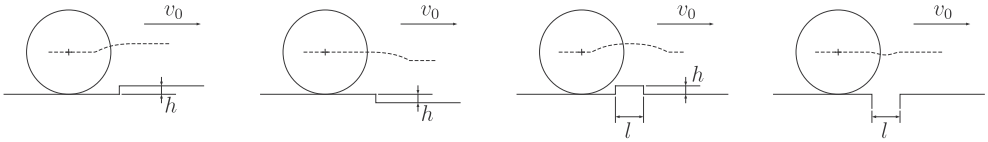


**Fig. 14.** Local defect shape (from left to right: step up, step down, positive pulse, negative pulse).

**Table 2**
AM96 train properties.

| | | $m_c$ [kg] | $I_c$ [kgm$^2$] | $m_b$ [kg] | $I_b$ [kgm$^2$] | $m_w$ [kg] | $k_1$ [MN/m] | $d_1$ [kNs/m] | $k_2$ [MN/m] | $d_2$ [kNs/m] |
|---|---|---|---|---|---|---|---|---|---|---|
| AM 96 | HVB | 25200 | $1.26 \times 10^6$ | 6900 | $1.52 \times 10^3$ | 1700 | 1.3 | 3.7 | 0.69 | 22.6 |
| | HVADX | 28900 | $1.45 \times 10^6$ | 7050 | $1.58 \times 10^3$ | 1700 | 1.3 | 3.7 | 0.69 | 22.6 |
| | HVBX | 25930 | $1.3 \times 10^6$ | 11800 | $2.6 \times 10^3$ | 1700 | 1.81 | 1.14 | 0.69 | 14 |
| Classic tram | | 7580 | $8.75 \times 10^4$ | 3530 | $6.0 \times 10^2$ | 160 | 5.876 | 6 | 0.96 | 56.25 |

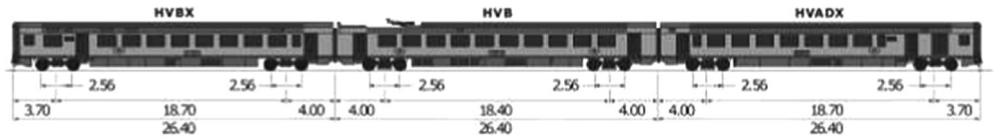


**Fig. 15.** AM96 train dimensions.

threshold running RMS value of 72 dB or 75 dB depending on the intended use of the building. The frequency content of the response is also below, k = 1.4, that is the limit for residential buildings during the night [59].

Next, the influence of defect type on building vibrations is analysed for both the AM96 train and the classic tram considering several defect types (Fig. 14). Fig. 19 presents the building response due to the AM96 passage over a ballasted track. Overall it can be

**Table 3**
Ballasted track properties.

| **Ballast track properties (2 rails)** | |
|---|---|
| Track gauge [m] | 1.435 |
| Rail 2nd moment of area [$m^4$] | $3.09 \times 10^{-5}$ |
| Rail Young's modulus [$N/m^2$] | $2.1 \times 10^{11}$ |
| Rail density [$kg/m^3$] | 7850 |
| Railpad stiffness per unit length (2 rails) [$N/m^2$] | $6.15 \times 10^{8}$ |
| Railpad damping per unit length (2 rails) [$Ns/m^2$] | $1.2 \times 10^{4}$ |
| Sleeper spacing [m] | 0.65 |
| Sleeper mass per unit length [kg/m] | 461.5 |
| Ballast stiffness [$N/m^2$] | $1.3 \times 10^{8}$ |
| Ballast damping [$Ns/m^2$] | $1.3 \times 10^{5}$ |
| Ballast density [$kg/m^3$] | 1700 |
| Ballast height (below sleeper) [m] | 0.3 |
| Ballast cross-sectional area [$m^2$] | 0.59 |
| Ballast Poisson's ratio | 0.3 |

**Table 4**
Slab track properties.

| Slab track properties (2 rails) | |
|---|---|
| Track gauge [m] | 1.435 |
| Rail 2nd moment of area [$m^4$] | $3.09 \times 10^{-5}$ |
| Rail Young's modulus [$N/m^2$] | $2.1 \times 10^{11}$ |
| Rail density [$kg/m^3$] | 7850 |
| Railpad stiffness per unit length (2 rails) [$N/m^2$] | $4 \times 10^{8}$ |
| Railpad damping per unit length (2 rails) [$Ns/m^2$] | $1.2 \times 10^{4}$ |
| Slab thickness [m] | 0.3 |
| Slab width [m] | 2.5 |
| Slab stiffness (concrete)[$N/m^2$] | $3 \times 10^{10}$ |
| Slab 2nd moment of area [$m^4$] | $5.63 \times 10^{-3}$ |
| Slab density (concrete) [$kg/m^3$] | 2500 |
| Slab Poison's ratio (concrete) | 0.2 |

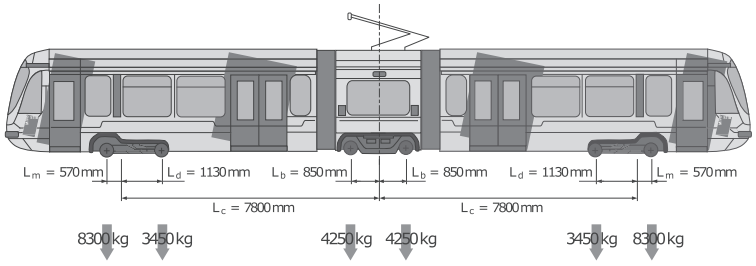


**Fig. 16.** Geometrical configuration of the classic tram.

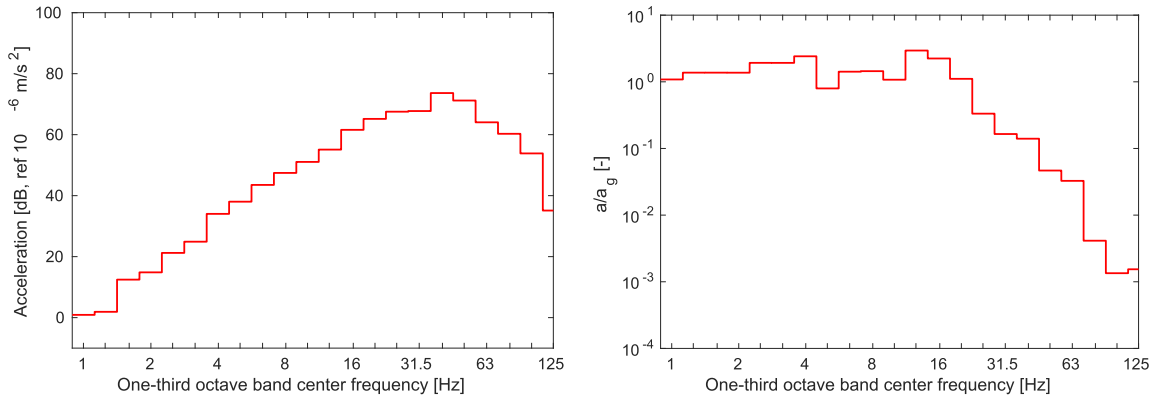


**Fig. 17.** (a) One-third octave band center frequency of the vertical acceleration of the free field response $a_g$ at 20 m to the ballasted track due to a AM96 train passage at $v_0 = 120$ km/h and (b) soil-structure transfer function $a/a_g$ at the top floor of a six-storey building.

observed the step up joint induces higher vibrations at low frequencies, whereas the maximum values at mid and high frequencies are due to the positive pulse. Also the defect type influences the amplitude of the response more dominantly than the shape (Fig. 19. (a)). These results are consistent with the corresponding free field responses due to local defects, accounting for the fact that the building transfer function is the same in all cases. The running RMS values (Fig. 19. (b)) have the following maximum amplitudes: 61.8, 61.9, 62.9 and 64 dB for negative pulse, positive pulse, step down and step up, respectively. The maxima do not show a clear dependency on the defect type because the responses have similar amplitudes. The building vibrations induced by the classic tram passage over a slab track can be observed in Fig. 20. The frequency responses show a similar tendency for all defect types. However, it is more clearly shown in the running RMS curves (Fig. 20. (b)) that the highest responses are found for the positive pulse and the step up joint. This is because the response (Fig. 20. (a)) for both defect types yields similar magnitudes in the dominant frequency range from 8 Hz to 20 Hz. In this case, the free-field vibration is concentrated at the natural frequencies of the structure, but the vibration level doesn't exceed the limits indicated in standards. The maximum RMS value reaches 70 dB and the frequency content is below the k = 1.4 curve.

In addition, the effect of defect size on building vibrations was studied for negative pulse defect lengths spanning $l = \{80, 110, 140, 170, 200\}$ mm. Fig. 21 shows the building response due to the classic tram passing over a slab track. The correlation between the response amplitude and the defect size is clearly observed in both the frequency and time domain curves. The level of vibration increases significantly with the defect size

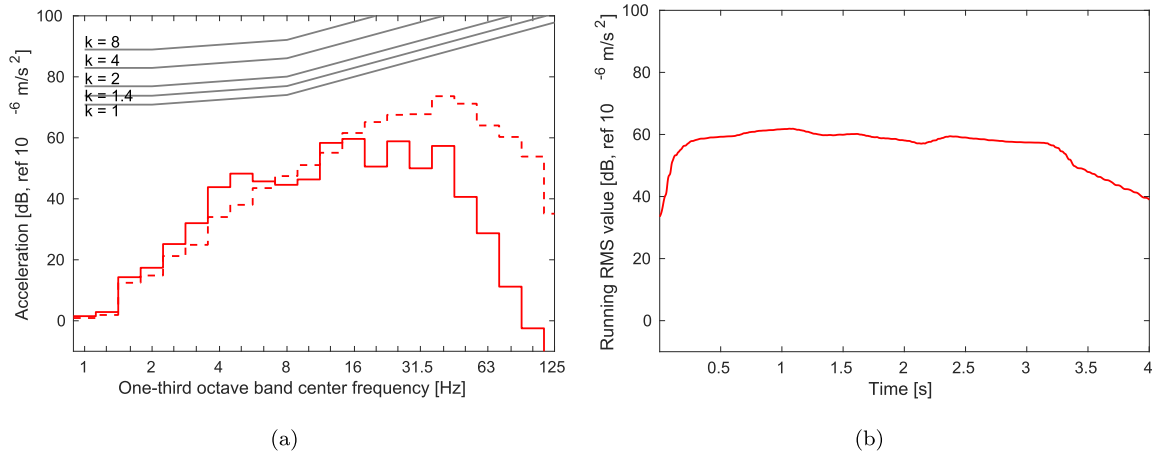


(a) (b)

**Fig. 18.** (a) One-third octave band center frequency of the $z$ vertical velocity and (b) running RMS value of the weighted acceleration at the top floor of the six-storey building due to a AM96 train passage at $v_0 = 120\,\text{km/h}$. The (dashed line) vertical acceleration of the free field response (Fig. 17. (a)) and the k-curves [59] are superimposed in (a).

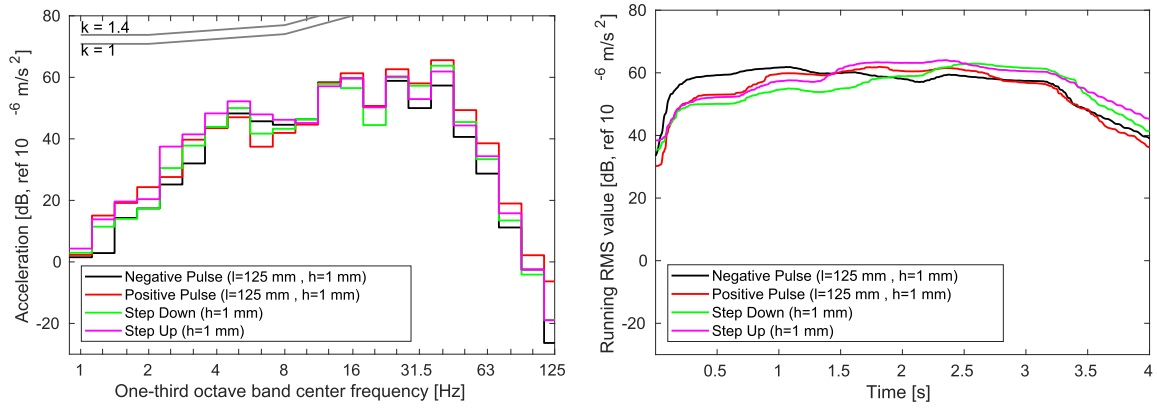


(a) (b)

**Fig. 19.** (a) One-third octave band center frequency of the $z$ vertical velocity and (b) running RMS value of the weighted acceleration at the top floor of the six-storey building for several defect types due to a AM96 train passage at $v_0 = 120\,\text{km/h}$. The k-curves [59] are superimposed in (a).

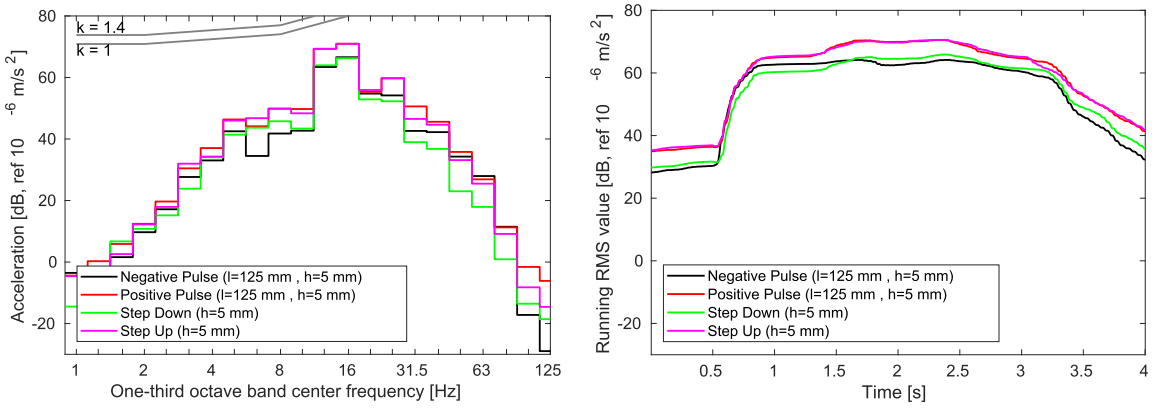


(a) (b)

**Fig. 20.** (a) One-third octave band center frequency of the $z$ vertical velocity and (b) running RMS value of the weighted acceleration at the top floor of the six-storey building for several defect types due to a tram passage at $v_0 = 40\,\text{km/h}$. The k-curves [59] are superimposed in (a).

from $l = 80$ to $l = 140\,\text{mm}$, whereas the building response increases slightly for higher values of defect size. Although the thresholds for human comfort are not exceeded, the levels are appreciable showing the importance of considering local track defects in addition to quasi-static and dynamic loads when computing building vibrations due to railway traffic. These cases could be studied by railway administrators in real cases to guarantee to inhabitants live comfortably.

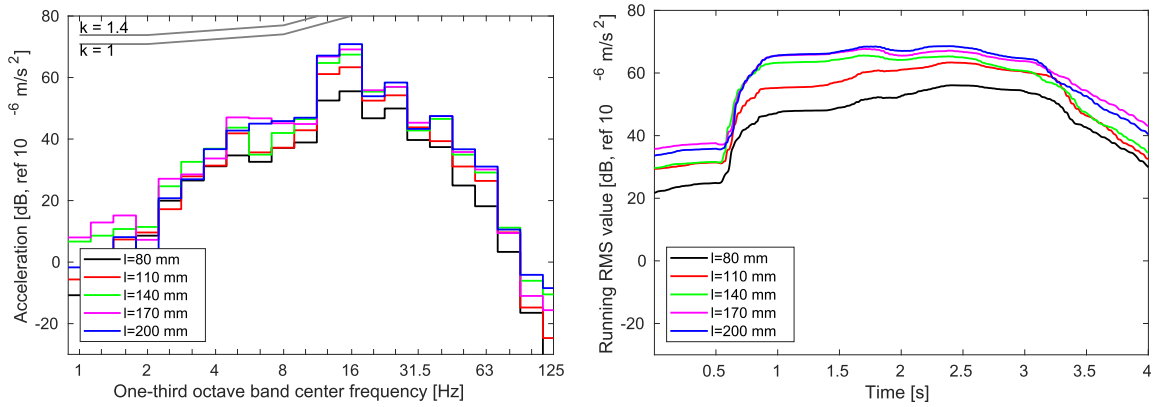


**Fig. 21.** (a) One-third octave band center frequency of the $z$ vertical velocity and (b) running RMS value of the weighted acceleration at the top floor of the six-storey building for several negative pulse defect sizes due to a tram passage at $v_0 = 40$ km/h. The k-curves [59] are superimposed in (a).

This section has shown the application of the proposed method to analyse building vibration due to railway defects. The performance of the transfer function method to predict building vibration provides a simple assessment once the ground borne vibration is obtained.

## 5. Conclusions

Building vibration induced by railway traffic is a problem that requires study during project planning and development phases. To do so, fast running methods are useful to assess building vibration quickly, considering multiple scenarios. In this work, a simplified method is presented to do this. It consists of a decoupled model, where the free-field vibration (source and propagation path) and the building vibration (receiver) are computed independently. The proposed model uses a soil-structure transfer function to characterise the structure and soil properties. This transfer function is then combined with the free-field response to obtain the building induced vibration in a computationally efficient manner.

The proposed method comprises four parts: (1) determination of the free-field vibration either numerically or experimentally (Fig. 2), (2) construction of a soil-building model that approximates SSI using a set of spring-damper elements (Fig. 4), (3) computation of the coupling loss and floor amplification factor of the building due to the incident wavefield, and finally, (4) summation of the results from parts (1) and (3) to compute the building response. The new model inherently characterises building response using both its transfer function and the free-field vibration. The transfer function depends upon the coupling loss and the floor amplification factors. The coupling loss induces an attenuation in the structural response in relation to the free-field response, that is dependent on frequency because attenuation is greater at higher frequencies. However, this factor can be approximated as a constant value, as used in standards [29–31] which propose an attenuation ranging from −13 dB (large masonry on spread footings) to 0 dB (foundation in rock). The attenuation computed from the proposed model is frequency dependent and lower than that in the standard, so should be used with care. In contrast, floor amplification can be approximated using a building model where the soil is neglected. This makes the problem more straightforward because SSI is then solely governed by the coupling loss factor.

The proposed methodology provides a significant computational saving compared to numerical approaches where the full modelling domain is solved for every single train passage. While the scoping model [45] has a computational time of 4 minutes and the SSIFiBo toolbox has a time of 3 − 9 hours, the newly proposed approach obtains the result instantly.

After the model is developed, the dynamic building response due to railway defects is studied. It is found that defect size has a strong influence on building vibrations and that these local track defects produce major vibration levels in buildings close to the railway line. The parametric study shows that local track defects can cause vibration levels close to the threshold of human comfort. The structural response is attenuated in the high frequency range due to the damping present in the free-field response and the building transfer function. The type of defect does not strongly influence on the building response, however, the defect size does. The vibration level increase from 56 dB to 65.6 dB for defect sizes of $l = 80$ and $l = 140$ mm, respectively. For even larger defect sizes, further vibration increases are marginal, up to 68.5 dB for a defect size of $l = 200$ mm. The discrepancies between ballasted and slab track vibration show that the type of track is an important parameter, which strongly affects free-field response [62]. Further, track irregularities dominate the free field response in the medium frequency range, and the significance of the quasi-static load is higher for the ballasted track.

The proposed methodology can be used to estimate the vibration in buildings, accounting for SSI and floor amplification, and the measured/computed free-field response due to railway traffic. The accuracy of the proposed model is within the uncertainty range found in previous research [63–65].

## Declaration of Competing Interest

The authors declare that they have no known competing financial interests or personal relationships that could have appeared to influence the work reported in this paper.

## Acknowledgements

The authors would like to acknowledge the financial support provided by the Spanish Ministry of Economy and Competitiveness (Ministerio de Economía y Competitividad) through research project BIA2016-75042-C2-1-R, Spanish Ministry of Education, Culture and Sport, Spain (Ministerio de Educación, Cultura y Deporte) through the scholarship "Salvador de Madariaga" Reference PRX18/00115, the Andalusian Scientific Computing Centre (CICA), the University of Leeds Cheney Award Scheme and the Leverhulme Trust (UK). They also acknowledge the support of Seville,

Mons and Leeds Universities, who, without their support, this research would not have been possible.

## References


[1] E. Kausel, Early history of soil-structute interaction, Soil Dyn. Earthquake Eng. 30 (2010) 822–8328, https://doi.org/10.1016/j.soildyn.2009.11.001.

[2] J. Wolf, Dynamic Soil-Structure Interaction, Prentice-Hall, Englewood Cliffs, New Jersey, 1985.

[3] C. Wu, H. Hao, Numerical study of characteristics of underground blast induced surface ground motion and their effect on above-ground structures. part i. ground motion characteristics, Soil Dyn. Earthquake Eng. 25 (2005) 27–38, https://doi.org/10.1016/j.soildyn.2004.08.001.

[4] H. Hao, C. Wu, Numerical study of characteristics of underground blast induced surface ground motion and their effect on above-ground structures. part ii. effects on structural responses, Soil Dyn. Earthquake Eng. 25 (2005) 39–53, https://doi.org/10.1016/j.soildyn.2004.08.002.

[5] A. Bayraktar, A. Can Altunis, M. Özcan, Safety assessment of structures for near-field blast-induced ground excitations using operational modal analysis, Soil Dyn. Earthquake Eng. 39 (2012) 23–36, https://doi.org/10.1016/j.soildyn.2012.02.005.

[6] O. Dogan, O. Anil, S.O. Akbas, E. Kantar, R.T. Erdem, Evaluation of blast-induced ground vibration effects in a new residential zone, Soil Dyn. Earthquake Eng. 50 (2013) 168–181, https://doi.org/10.1016/j.soildyn.2013.03.005.

[7] E. Savin, D. Clouteau, Elastic wave propagation in a 3-D unbounded random heterogeneous medium coupled with a bounded medium. application to seismic soil-structure interaction (sssi), Int. J. Numerical Methods Eng. 54 (2002) 607–630, https://doi.org/10.1002/nme.442.

[8] F. Gatti, S. Touhami, F. Lopez-Caballero, R. Paolucci, D. Clouteau, V.A. Fernandes, M. Kham, F. Voldoire, Broad-band 3-D earthquake simulation at nuclear site by an all-embracing source-to-structure approach, Soil Dyn. Earthquake Eng. 115 (2018) 263–280, https://doi.org/10.1016/j.soildyn.2018.08.028.

[9] R. Taherzadeh, D. Clouteau, R. Cottereau, Simple formulas for the dynamic stiffness of pile groups, Earthquake Eng. Struct. Dynam. 38 (2009) 1665–1685, https://doi.org/10.1002/eqe.918.

[10] D. Pitilakis, D. Clouteau, Equivalent linear substructure approximation of soil-foundation-structure interaction: model presentation and validation, Bull. Earthq. Eng. 8 (2) (2010) 257–282, https://doi.org/10.1007/s10518-009-9128-3.

[11] H. Torabi, M. Rayhani, Three dimensional finite element modeling of seismic soil-structure interaction in soft soil, Comput. Geotech. 60 (2014) 9–19, https://doi.org/10.1016/j.compgeo.2014.03.014.

[12] L. Pyl, G. Degrande, G. Lombaert, W. Haegeman, Validation of a source-receiver model for road traffic- induced vibrations in buildings. i: Source model, J. Eng. Mech. 130 (2004) 1377–1393, https://doi.org/10.1061/(ASCE)0733-9399(2004)130:12(1377).

[13] L. Pyl, G. Degrande, D. Clouteau, Validation of a source-receiver model for road traffic- induced vibrations in buildings. ii: Receiver model, J. Eng. Mech. 130 (2004) 1394–1406, https://doi.org/10.1061/(ASCE)0733-9399(2004)130:12(1394).

[14] S. François, L. Pyl, H. Masoumi, G. Degrande, The influence of dynamic soil-structure interaction on traffic induced vibrations in buildings, Soil Dyn. Earthquake Eng. 27 (2007) 655–674, https://doi.org/10.1016/j.soildyn.2006.11.008.

[15] D. Connolly, G. Marecki, G. Kouroussis, I. Thalassinakis, P. Woodward, The growth of railway ground vibration problems – A review, Sci. Total Environ. 568 (2015) 1276–1282, https://doi.org/10.1016/j.scitotenv.2015.09.101.

[16] G. Kouroussis, S. Zhu, B. Olivier, D.A.W. Zhai, Urban railway ground vibrations induced by localized defects: using dynamic vibration absorbers as a mitigation solution, J. Zhejiang University-Science A 20 (2) (2019) 83–97, https://doi.org/10.1631/jzus.A1800651.

[17] S. Zhu, J. Wang, C. Cai, K. Wang, W. Zhai, J. Yang, H. Yan, Development of a vibration attenuation track at low frequencies for urban rail transit, Computer-Aided Civil Infrastructure Eng. 32 (2017) 713–726, https://doi.org/10.1111/mice.12285.

[18] K. Vogiatzis, H. Mouzakis, Ground-borne noise and vibration transmitted from subway networks to multi-storey reinforced concrete buildings, Transport 33 (2) (2018) 446–453, https://doi.org/10.3846/16484142.2017.1347895.

[19] K. Vogiatzis, H. Mouzakis, V. Zafiropoulou, Assessing subway network ground borne noise and vibration using transfer function from tunnel wall to soil surface measured by muck train operation, Sci. Total Environ. 650 (2019) 2888–2896.

[20] G. Kouroussis, J. Florentin, O. Verlinden, Ground vibrations induced by intercity/interregion trains: a numerical prediction based on the multibody/finite element modeling approach, J. Vib. Control 22 (2016) 4192–4210, https://doi.org/10.1177/1077546315573914.

[21] International Organization for Standardization, ISO 2631-1:2003: Mechanical vibration and shock–Evaluation of human exposure to whole-body vibration–Part 1: General requirements (2003)..

[22] International Organization for Standardization, ISO 2631-2:2003: Mechanical vibration and shock–Evaluation of human exposure to whole-body vibration–Part 2: Vibration in buildings (1–80 Hz) (2003)..

[23] International Organization for Standardization, ISO 14837-1:2005 Mechanical vibration–Ground-borne noise and vibration arising from rail systems–Part 1: General guidance (2005)..

[24] P. Fiala, G. Degrande, F. Augusztinovicz, Numerical modelling of ground-borne noise and vibration in buildings due to surface rail traffic, J. Sound Vib. 301 (2007) 718–738, https://doi.org/10.1016/j.jsv.2006.10.019.

[25] P. Galvín, A. Romero, J. Domínguez, Fully three-dimensional analysis of high-speed train–track–soil–structure dynamic interaction, J. Sound Vib. 329 (2010) 5147–5163, https://doi.org/10.1016/j.jsv.2010.06.016.

[26] D. Cantero, T. Arvidsson, E. OBrien, R. Karoumi, Train-track-bridge modelling and review of parameters, Struct. Infrastructure Eng. 12 (9) (2016) 1051–1064, https://doi.org/10.1080/15732479.2015.1076854.

[27] A. Doménech, M. Martínez-Rodrigo, A. Romero, P. Galvín, On the basic phenomenon of soil-structure interaction on the free vibration response of beams: Application to railway bridges, Eng. Struct. 125 (2016) 254–265, https://doi.org/10.1016/j.engstruct.2016.06.052.

[28] P. Coulier, G. Lombaert, G. Degrande, The influence of source-receiver interaction on the numerical prediction of railway induced vibrations, J. Sound Vib. 333 (2014) 2520–2538, https://doi.org/10.1016/j.jsv.2014.01.017.

[29] C.E. Hanson, D.A. Towers, L.D. Meister, High-speed ground Transportation Noise and Vibration Impact Assessment, HMMH Report 293630-4, U.S. Department of Transportation, Federal Railroad Administration, Office of Railroad Development..

[30] C.E. Hanson, D.A. Towers, L.D. Meister, Transit Noise and Vibration Impact Assessment, Report FTA-VA-90-1003-06, U.S. Department of Transportation, Federal Transit Administration, Office of Planning and Environment..

[31] Federal Railroad Administration, High-Speed Ground Transportation Noise and Vibration Impact Assessment, U.S. Department of Transportation (2012)..

[32] W. Rücker, L. Auersch, A user-friendly prediction tool for railway induced ground vibrations: Emission - transmission - immission, Notes Numer. Fluid Mech. Multidisciplinary Design 99 (2008) 129–135, https://doi.org/10.1007/978-3-540-74893-9_18.

[33] L. Auersch, Dynamic stiffness of foundations on inhomogeneous soils for a realistic prediction of vertical building resonance, J. Geotechnical Geoenvironmental Eng. 134 (3) (2008) 328–340, https://doi.org/10.1061/(ASCE)1090-0241(2008)134:3(328).

[34] L. Auersch, Building response due to ground vibration-simple prediction model based on experience with detailed models and measurements, Int. J. Acoustics Vib. 15 (3) (2010) 101–112, https://doi.org/10.20855/ijav.2010.15.3262.

[35] L. Auersch, Wave propagation in the elastic half-space due to an interior load and its application to ground vibration problems and buildings on pile foundations, Soil Dyn. Earthquake Eng. 30 (2010) 925–936, https://doi.org/10.1016/j.soildyn.2010.04.003.

[36] M. Hussein, H. Hunt, K. Kuo, P. Alves Costa, J. Barbosa, The use of sub-modelling technique to calculate vibration in buildings from underground railways, Proc. Inst. Mech. Eng., Part F 229 (3) (2013) 303–314, https://doi.org/10.1177/0954409713511449.

[37] M. Hussein, H. Hunt, K. Kuo, P. Alves Costa, J. Barbosa, The dynamic effect of piled-foundation building on an incicident vibration field from an underground railway tunnel, in: 20th International Congress on Sound & Vibration. ICSV 20..

[38] G. Kouroussis, L.V. Parys, C. Conti, O. Verlinden, Prediction of ground vibrations induced by urban railway traffic: An analysis of the coupling assumptions between vehicle, track, soil, and buildings, Int. J. Acoust. Vib. 18 (4) (2013) 163–172, https://doi.org/10.20855/ijav.2013.18.4330.

[39] G. Kouroussis, K.E. Vogiatzis, D.P. Connolly, A combined numerical/experimental prediction method for urban railway vibration, Soil Dyn. Earthquake Eng. 97 (2017) 377–386, https://doi.org/10.1016/j.soildyn.2017.03.030.

[40] G. Kouroussis, K.E. Vogiatzis, D.P. Connolly, Assessment of railway ground vibration in urban area using in-situ transfer mobilities and simulated vehicle-track interaction, Int. J. Rail Transp. 6 (2018) 113–130, https://doi.org/10.1080/23248378.2017.1399093.

[41] P. Lopes, P. Alves Costa, M. Ferraz, R. Calçada, A. Silva Cardoso, Numerical modeling of vibrations induced by railway traffic in tunnels: From the source to the nearby buildings, Soil Dyn. Earthquake Eng. 61–62 (2014) 269–285, https://doi.org/10.1016/j.soildyn.2014.02.013.

[42] P. Lopes, J. Fernández Ruiz, P. Alves Costa, L. Medina Rodríguez, A. Silva Cardoso, Vibrations inside buildings due to subway railway traffic. experimental validation of a comprehensive prediction model, Science of the Total, Environment 568 (2016) 1333–1343, https://doi.org/10.1016/j.scitotenv.2015.11.016.

[43] D.P. Connolly, G. Kouroussis, A. Giannopoulos, O. Verlinden, P.K. Woodward, M.C. Forde, Assesment of railway vibrations using an efficient scoping model, Soil Dyn. Earthquake Eng. 58 (2014) 37–47, https://doi.org/10.1016/j.soildyn.2013.12.003.

[44] D.P. Connolly, G. Kouroussis, P.K. Woodward, A. Giannopoulos, O. Verlinden, M.C. Forde, Scoping prediction of re-radiated ground-borne noise and vibration near high speed rails lines with variable soils, Soil Dyn. Earthquake Eng. 66 (2014) 78–88, https://doi.org/10.1016/j.soildyn.2014.06.021.

[45] D. López-Mendoza, A. Romero, D. Connolly, P. Galvín, Scoping assessment of building vibration induced by railway traffic, Soil Dyn. Earthquake Eng. 93 (2017) 147–161, https://doi.org/10.1016/j.soildyn.2016.12.008.

[46] K. Kuo, M. Papadopoulos, G. Lombaert, G. Degrande, The coupling loss of a building subject to railway induced vibrations: Numerical modelling and experimental measurements, J. Sound Vib. 442 (2019) 459–481, https://doi.org/10.1016/j.jsv.2018.10.048.
[47] D.P. Connolly, P. Galvín, B. Olivier, A. Romero, G. Kouroussis, A 2.5D time-frequency domain model for railway induced soil-building vibration due to railway defects, Soil Dyn. Earthquake Eng. 120 (2019) 332–344, https://doi.org/10.1016/j.soildyn.2019.01.030.
[48] O. Zienkiewicz, The Finite Element Method, 3rd Edition., McGraw-Hill, 1986.
[49] N. Newmark, A method of computation for structural dynamics, ASCE J. Eng. Mech. Division 85 (1959) 67–94.
[50] R. Clough, J. Penzien, Dynamic of Structures, McGraw-Hill, New York, 1975.
[51] National Institute of Standards and Technology U.S. Department of Commerce, NIST GCR 12-917-21 Soil-Structure Interaction for Building Structures (2012)..
[52] A. Pais, E. Kausel, Approximate formulas for dynamic stiffness of rigid foundations, Soil Dyn. Earthquake Eng. 7 (4) (1988) 213–227, https://doi.org/10.1016/S0267-7261(88)80005-8.
[53] European Committee for Standardization, Eurocode 8: Design of structures for earthquake resistance–Part 1: General rules, seismic actions and rules for buildings (1998)..
[54] P. Galvín, D. Mendoza, D. Connolly, G. Degrande, G. Lombaert, A. Romero, Scoping assessment of free-field vibrations due to railway traffic, Soil Dyn. Earthquake Eng. 114 (2018) 598–614, https://doi.org/10.1016/j.soildyn.2018.07.046.
[55] A. Romero, P. Galvín, A bem-fem using layered half-space green's function in time domain for ssi analyses, Eng. Anal. Boundary Elem. 55 (2015) 93–103, https://doi.org/10.1016/j.enganabound.2014.11.027. coupling Techniques.
[56] D. López-Mendoza, A. Romero, D. Connolly, P. Galvín, Scoping assessment of building vibration induced by railway traffic, Soil Dyn. Earthquake Eng. 93 (2017) 147–161, https://doi.org/10.1016/j.soildyn.2016.12.008.
[57] P. Galvín, A. Romero, A MATLAB toolbox for soil-structure interaction analysis with finite and boundary elements, Soil Dyn. Earthquake Eng. 57 (2014) 10–14, https://doi.org/10.1016/j.soildyn.2013.10.009.
[58] Deutsches Institut für Normung, DIN 45672 Teil 2: Schwingungsmessungen in der Umgebung von Schienenverkehrswegen: Auswerteverfahren (1995)..
[59] International Organization for Standardization, ISO 2631-2:1989: Mechanical vibration and shock–Evaluation of human exposure to whole-body vibration–Part 2: Vibration in buildings (1–80 Hz) (2003)..
[60] G. Kouroussis, D.P. Connolly, K.E. Vogiatzis, O. Verlinden, Modelling the environmental effects of railway vibrations from different types of rolling stock: a numerical study, Shock Vib. 6 (2015), https://doi.org/10.1155/2015/142807.
[61] Ministerio de la Presidencia de España, Ley 37/2003 del Ruido (2007)..
[62] P. Galvín, A. Romero, J. Domínguez, Vibrations induced by hst passage on ballast and non-ballast tracks, Soil Dyn. Earthquake Eng. 30 (9) (2010) 862–873.
[63] G. Lombaert, P. Galvín, S. François, G. Degrande, Quantification of uncertainty in the prediction of railway induced ground vibration due to the use of statistical track unevenness data, J. Sound Vib. 333 (18) (2014) 4232–4253, https://doi.org/10.1016/j.jsv.2014.04.052.
[64] S. Jones, K. Kuo, M.F.M. Hussein, H.E.M. Hunt, Prediction uncertainties and inaccuracies resulting from common assumptions in modelling vibration from underground railways, Proc. Inst. Mech. Eng., Part F 226 (2012) 501–512, https://doi.org/10.1177/0954409712441744.
[65] D.P. Connolly, P. Alves Costa, G. Kouroussis, Large scale international testing of railway ground vibrations across Europe, Soil Dynamics and Earthquake Engineering 71 (2015) 1–12, https://doi.org/10.1016/j.soildyn.2015.01.001.